Available online at www.sciencedirect.com
SCIENCE DIRECT
International Journal of Multiphase Flow 32 (2006) 553–567
International Journal of Multiphase Flow
www.elsevier.com/locate/ijmulflow

An inverse dispersed multiphase flow model for liquid production rate determination

S. Guet [a,*], O.M.H. Rodriguez [a], R.V.A. Oliemans [a], N. Brauner [b]

[a] *Kramers Laboratorium, J.M. Burgers Centre for Fluid Mechanics, Delft University of Technology, Prins Bernhardlaan 6, 2628 BW Delft, The Netherlands*
[b] *School of Engineering, Tel-Aviv University, Tel-Aviv 69978, Israel*

Received 9 August 2005; received in revised form 19 January 2006

Abstract

The aim of this study is to develop a model for the determination of the superficial velocities in horizontal and slightly inclined oil–water pipe flow conditions by using pressure gradient and mixture density information. In this article an inverse model is suggested for a dispersion of oil in water and of water in oil. This approach permits to select dispersed flow conditions from a set of experimental data, and uses a new hybrid model for the effective viscosity. A set of 310 oil–water experimental data points collected on an experimental set-up of length $L = 15$ m and diameter $D = 8.28$ cm at various (slight) orientations is used to validate the inverse method. The comparison between model reconstructions and measured flow velocities show a reasonable agreement.

Keywords: Liquid–liquid flow; Inverse model; Dispersed regime; Effective viscosity; Drop size

1. Introduction

In the oil industry, very often a number of pipes are connected via T-junctions in under-sea or under ground configurations. These pipelines are producing from different oil reservoirs with different intake pressure and water cut conditions. Current technologies have shown that pressure and mixture density determination are possible on these pipelines by using piezo-electric and gamma-ray measurement techniques. However, the in situ determination of the oil and water flow rate remains an important issue, since available flow rate measurement techniques would be difficult to install in such situations. In the present research project we want to develop a method for computing the oil and water superficial velocities based on pressure gradient and

* Corresponding author. Present address: Institut Français du Pétrole, 3-4 Avenue de Bois-Préau, 92500 Rueil Malmaison, France.
E-mail addresses: s.c.l.guet@wbmt.tudelft.nl, sebastien.guet@ifp.fr (S. Guet).

0301-9322/$ - see front matter © 2006 Elsevier Ltd. All rights reserved.
doi:10.1016/j.ijmultiphaseflow.2006.01.008

mixture density information in horizontal and slightly inclined oil–water flows. The objective of this article is to propose an inverse mode calculation model for dispersed flow conditions, and to compare the model predictions with experimental data. Two main subjects will be studied: (1) the flow pattern transition from stratified to fully dispersed flow regime, and (2) dispersed flow regime pressure gradient modelling. An inverse model able to select data pertaining to dispersed flow conditions and to reconstruct the associated superficial velocities will be suggested and tested.

A set of experimental data collected on a horizontal and slightly inclined pipe flow of diameter, $D = 82.8$ mm and length $L = 15$ m is used for validation purpose (Rodriguez and Oliemans, 2006). These data were collected on the Donau multiphase flow loop in Shell Rijswijk, the Netherlands. The oil used in this study has a density of 830 kg m^{-3} and a viscosity $\mu_o = 7.5$ mPa s. The water has a density of 1060 kg m^{-3} and a viscosity $\mu_w = 0.8$ mPa s. The pressure gradient, oil and water volumetric flow rate, temperature, as well as the mixture density were measured. The techniques used for this purpose were: pressure differential meters, thermocouples, and gamma-ray densitometry. Various angles of inclination were investigated ($\beta = -5$, -2, -1.5, 0, 1, 2, and 5°.) Also movies of each of the 310 experimental data points were taken, allowing for the flow pattern determination. The reader is referred to van Kemenade et al. (2003) for a general description of the Donau flow loop multiphase flow set-up and to Rodriguez and Oliemans (2006) for a more detailed description of the oil water experiments.

In the dispersed flow regime, it is common to use a homogeneous no-slip model to compute the frictional pressure gradient. The mixture is therefore considered as a single fluid with an equivalent mixture density ρ_m and an effective viscosity μ_m, and a model taken from single phase flow is applied for the friction factor. The model used for the effective viscosity is then critical for a proper determination of the frictional pressure gradient. Depending on the flow conditions and fluid properties, a number of models have been suggested in the literature (Pal, 2001; Brauner, 1998; Elseth, 2001). It was shown previously by Rodriguez and Oliemans (2006), that the pressure gradient data collected at dispersed flow conditions could be described reasonably by using an homogeneous no slip model. However, the prediction of the pressure gradient for w/o (dispersion of water in oil) were not as accurate as for o/w (dispersion of oil in water), and the suggested model was tested in the frame of a direct model with the à priori knowledge of the flow pattern. In this respect, it is of interest to check how an inverse modelling approach would perform.

In the present study we will assume that single phase flow friction factor correlations can be applied to dispersed two-phase flows. The collected experimental data will be used to extract flow pattern, as well as effective viscosity information from the pressure gradient measurements. Since the appropriate modelling method depends on the flow pattern conditions (dispersed flow, stratified flow, etc.), a physically based model is implemented for predicting the transition to fully dispersed flow based on the approach described in Brauner (2001) (Section 2). This model will be extended to take into account the effect of wall roughness, frequently encountered in practice. Particular attention will be paid to the possibility of using this approach via a simple set of equations, which are potentially easy to implement in the inverse problem.

Dispersed flow regime experimental data will be selected from our total set of 310 experiments. These 90 selected data points collected at various inclination angles will be used to infer appropriate effective viscosity models for the dispersed flow regime. Data from the literature (Fairusov et al., 2000; Elseth, 2001) as well as the present measurements will then be used for validating the flow pattern boundaries. Pressure gradient predictions will then be presented. Finally, an inverse model able to select dispersed flow regime data and to reconstruct the associated oil and water superficial velocities on the basis of pressure gradient and mixture density information will be formulated. This model will be tested on the experimental data.

This paper is organised as follows: first, the model for the transition to full liquid–liquid dispersion is summarized and is compared with experimental data in Sections 2 and 3. Then the water-cut data are briefly discussed (Section 4). In Section 5, the pressure gradient measurements are used to obtain effective viscosity data in dispersed flow conditions. A new effective viscosity model is suggested based on these results (Section 6). The results for the pressure gradient predictions are then compared with the measurements (Section 7). An inverse method is suggested for the reconstruction of the superficial velocities, based on the suggested effective viscosity model. Reconstructed superficial velocities are compared with the direct measurements in Section 8.

2. Dispersed flow boundary modelling

For modelling the boundaries to dispersed flow, the model of Brauner (2001) is used and extended to take into account the effects of wall roughness (Section 2.1 and Appendix A). The determination of the continuous phase is made by applying a model for the critical water cut at phase inversion (Section 2.2).

2.1. Transition from separated to dispersed flow

The system Eötvös number corresponding to our experiments is $Eo_D = \frac{\Delta\rho g D^2}{8\sigma} \approx 35$. Here σ is the oil–water surface tension, $\Delta\rho = \rho_w - \rho_o$ is the difference of fluid densities and D is the pipe diameter. For such flow conditions ($Eo_D > 5$), the dispersed flow regime transition boundaries can be described by the model developed in Brauner (2001). This model is given by the criterion $d_{max} = d_{crit}$, where d_{max} is the maximum drop size existing in the system (due to turbulence break-up and eventually coalescence) and d_{crit} corresponds to the critical drop size above which the drop size is not stabilized, i.e., the drops are either deformed due to surface tension effects or are migrating toward the tube walls.

In the present work the model suggested by Brauner (2001) is applied and extended to take into account the effects of wall roughness onto the maximum drop size. This is implemented by using the wall roughness dependent correlation of Haaland (1983) for the friction factor:

$$f = \left[-1.8\log_{10}\left(\frac{6.9}{Re_m} + \left(\frac{e}{3.7D}\right)^{1.1}\right)\right]^{-2}, \tag{1}$$

where e is the wall equivalent roughness. $Re_m = \frac{U_m \rho_m D}{\mu_m}$ is the mixture Reynolds number, U_m and ρ_m are the mixture velocity and density, and μ_m is an effective viscosity. By using relation (1) we assume that single phase flow friction factor expressions can be applied in two phase dispersed flow conditions.

In our model, for a given value of the dispersed phase volume fraction the regime is determined as dispersed flow when the mixture velocity is above a critical value, which corresponds to $d_{max} = d_{crit}$. Using this approach, the boundaries between separated and dispersed flow are computed as combinations of critical superficial oil and water velocities. More details about the mathematical formulation of our dispersed flow transition model are given in Appendix A.

2.2. Continuous phase determination

The transition from water continuous dispersion to oil continuous dispersion is determined by using the correlation suggested by Arirachakaran et al. (1989) for the value of the critical water cut $C_w = C_{w,crit}$ at transition:

$$C_{w,crit} = 0.5 - 0.1108\log_{10}\left(\frac{\mu_o}{\mu_w}\right), \tag{2}$$

where μ_o and μ_w are the oil and water viscosity and the water cut is defined as a ratio of the water superficial velocity and the mixture velocity, $C_w = \frac{U_{sw}}{U_m}$. It can be noted that other relations are available for the critical water cut at phase inversion. Based on various collected experiments, Brauner and Ullmann (2002) suggested the use of a best fit relation $C_{w,crit} = \frac{\left(\frac{\mu_o}{\mu_w}\right)^{0.22}}{1+\left(\frac{\mu_o}{\mu_w}\right)^{0.22}}$. For our range of fluid viscosities, these two models provide similar results ($0.36 < C_{w,crit} < 0.4$), therefore the final model is not strongly affected by the chosen correlation. Recent contributions have also outlined an impact of the fluid velocities on the critical water cut corresponding to phase inversion, due to the relative importance of turbulence in the two phases (Decarre and Fabre, 1997; Brauner and Ullmann, 2002). In the present model, this effect is neglected.

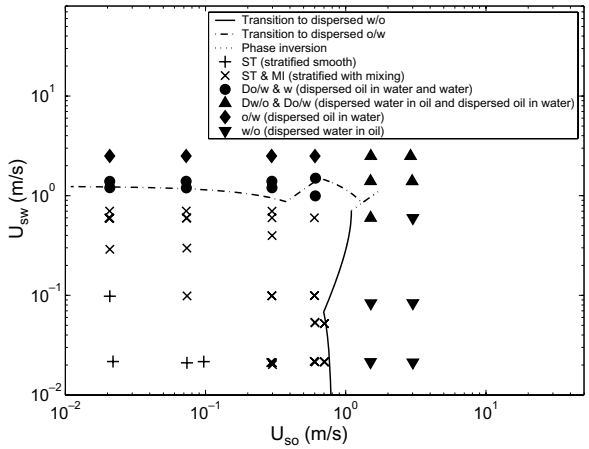

Fig. 1. Boundaries to finely dispersed liquid–liquid flows using our model for the transition to dispersed flow conditions. Experiments of Rodriguez and Oliemans (2006) for a horizontal pipe of diameter $D = 82.8$ mm, with a wall roughness $e = 10^{-5}$ m. The oil properties are $\mu_0 = 7.5$ mPa s and $\rho_0 = 830$ kg m^{-3}. The closed symbols refer to dispersed flow (Do/w&w, Dw/o&Do/w, o/w and w/o).

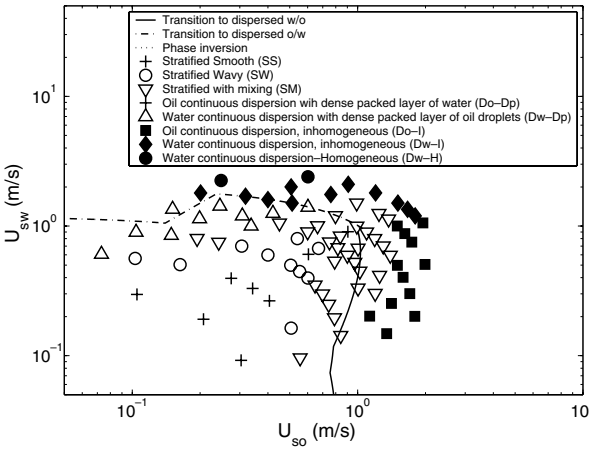

Fig. 2. Experiments of Elseth (2001) for a horizontal pipe of diameter $D = 56.3$ mm and roughness $e = 10^{-5}$ m. The oil properties are $\mu_0 = 1.64$ mPa s, $\rho_0 = 790$ kg m^{-3} and the surface tension is $\sigma = 43$ mN m^{-1}. Also our predictions for the transition to dispersed flow are displayed. The closed symbols refer to dispersed flow (Do-I, Dw-I, and Dw-H). The patterns (Do-Dp) and (Dw-Dp) are associated with the region of transition from separated to dispersed flow.

3. Comparison with experimental data

3.1. Flow pattern map

In Fig. 1 the boundaries to finely dispersed liquid–liquid flows corresponding to our fluid and set-up properties are shown. Also our analyzed experimental data corresponding to an angle of orientation $\beta = 0$ (i.e., horizontal flow) are shown. The distinction between o/w and w/o was not obvious when analysing the digitalised films, making the detection of phase inversion a difficult task. The presence of stratified flow and dispersed flow could however be determined without such ambiguities.

We also compared the predictions for the transition to fully dispersed regime with experimental data collected for other pipe diameter values. The results for the comparison with a smaller diameter, smooth pipe by Elseth (2001) and for a large diameter rough pipe by Fairusov et al. (2000) are displayed in Figs. 2 and 3, respectively. To compare with the data of Elseth (2001), we used the model with $e = 10^{-5}$ m in Fig. 2 (the

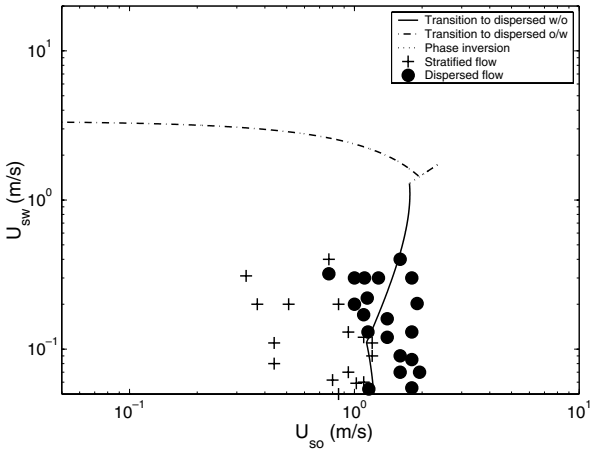

Fig. 3. Experiments of Fairusov et al. (2000) for a horizontal pipe of diameter $D = 363.5$ mm. The oil properties are $\mu_o = 5$ mPa s, $\rho_o = 851$ kg m^3 and the surface tension is $\sigma = 36$ mN m^{-1}. Our predictions for the transition to dispersed flow are displayed. The pipe roughness value reported by the authors ($e = 7 \times 10^{-5}$ m) is used in the calculations. The closed circles represent dispersed flow.

author used a Perspex pipe). For the comparison with the experimental data of Fairusov et al. (2000), we used the model with an equivalent roughness $e = 7.10^{-5}$ m, as reported by the author. As can be seen from the comparisons, the model permits to correctly predict the transition to dispersed flow. The use of the relation of Haaland (1983) for taking into account wall roughness effects also improved the predictions for smooth wall experiments, as it better represents the variations of the friction factor over a wide range of *Re* number.

Since our experiments are carried out at varied angle of orientation β from the horizontal ($-5 < \beta < +5°$), it is interesting to look at the changes in the flow pattern map when varying the angle β. We therefore also investigated this effect with our model: no significant changes were found for slight pipe orientation angles with respect to the horizontal ($-15 < \beta < +15°$, in which β is defined as positive for upward flow).

4. Hold-up data

Mixture density data were collected via a gamma-densitometer, allowing for the determination of the hold-up. To verify the validity of these mixture density measurements, a comparison can be made with an estimate of the mixture density obtained by using the volumetric flow rate measurements: assuming validity of the no-slip homogeneous model, the water volumetric concentration can be estimated by

$$\epsilon_w = C_w = \frac{U_{sw}}{U_{so} + U_{sw}}, \tag{3}$$

and the mixture density is given by

$$\rho_m = C_w \rho_w + (1 - C_w)\rho_o. \tag{4}$$

A comparison of the mixture density as measured by the gamma densitometer and that obtained by using this approach was made in Rodriguez and Oliemans (2006). It was shown that, indeed, this formulation is valid for dispersed flow conditions corresponding to w/o (dispersion of water in oil), o/w (dispersion of oil in water), Dw/o&Do/w (dispersion of water in oil and dispersion of oil in water) as well as Do/w&w (dispersion of oil in water and water). We selected dispersed flow conditions by using our flow pattern transition model. We then made a comparison between the gamma-ray measurements and the homogeneous model method. Using Eq. (4) leads to a maximum deviation of less than $\pm 3\%$ on the mixture density determination.

5. Effective viscosity estimates

In dispersed flow regime conditions, making predictions of the pressure gradient asks for the validation of an effective viscosity model. Provided the flow is fully dispersed, the frictional pressure gradient is given by

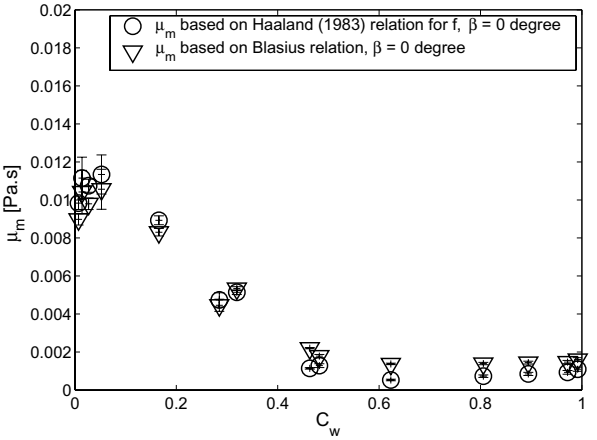

Fig. 4. Mixture viscosity estimates based on the measured frictional pressure gradient on the pipe flow, for $\beta = 0°$. Both the Blasius relation for smooth wall and the relation suggested by Haaland (1983) are used to compute the effective viscosity.

$$\left[\frac{\partial P}{\partial z}\right]_f = \frac{f \rho_m U_m^2}{2D}. \tag{5}$$

The friction factor f is given by Blasius relation for a smooth tube, $f = 0.316/Re_m^{0.25}$. The relation of Haaland (1983) is used for taking into account wall roughness effects (relation (1)). Based on the friction factor expressions of Blasius and of Haaland (1983), the effective viscosity μ_m (needed for calculating the Reynolds number Re_m) can be estimated by using the measured pressure gradients. This is done numerically by solving Eq. (5) with either Blasius relation or Eq. (1) for each measurement. It should be kept in mind, however, that for large roughness of the pipe wall the influence of the effective viscosity on the pressure gradient becomes negligible (see Eq. (1)). Therefore, only low and moderately low pipe roughness data can be used for effective viscosity estimates with our approach. For our experimental data the equivalent roughness of the pipe wall corresponds to 'smooth' Perspex pipe values ($e = 10^{-5}$ m), therefore these data are appropriate for extracting effective viscosity information.

The results are displayed in Fig. 4 for the experiments carried out at $\beta = 0°$ and when operating in the dispersed regime ($U_{sc} > 1.5$ m/s). A similar behaviour is obtained when analyzing experiments carried out at non-zero orientation angle β. However, for inclined flow experiments the scatter in the evaluated mixture viscosity data was found to be more pronounced. This can be attributed to a number of effects. In particular, during these tests the gravitational pressure gradient has to be estimated and used to compute the frictional pressure gradient:

$$\left[\frac{\partial P}{\partial z}\right]_f = \left[\frac{\partial P}{\partial z}\right]_{\text{measured}} - \left[\frac{\partial P}{\partial z}\right]_g, \tag{6}$$

where the gravitational pressure gradient is estimated as $\left[\frac{\partial P}{\partial z}\right]_g = \rho_m g \sin\beta$ and ρ_m is computed on the basis of the homogeneous no-slip model (relation (4)). This extra calculation implies that the effective viscosity values are less accurate for inclined flow situations.

6. Effective viscosity modelling

In Fig. 5a and b, the obtained effective viscosity data are compared with a number of available models (see Brauner (1998) and Becher (2001) for an overview of these models):

1. $\mu_m = (1 + 2.5\epsilon_d)\mu_c$, as derived by Einstein (1906). This relation is valid for low dispersed phase fraction;
2. $\mu_m = (1 + 4.5\epsilon_d)\mu_c$, valid for higher concentrations (Brauner, 1998);

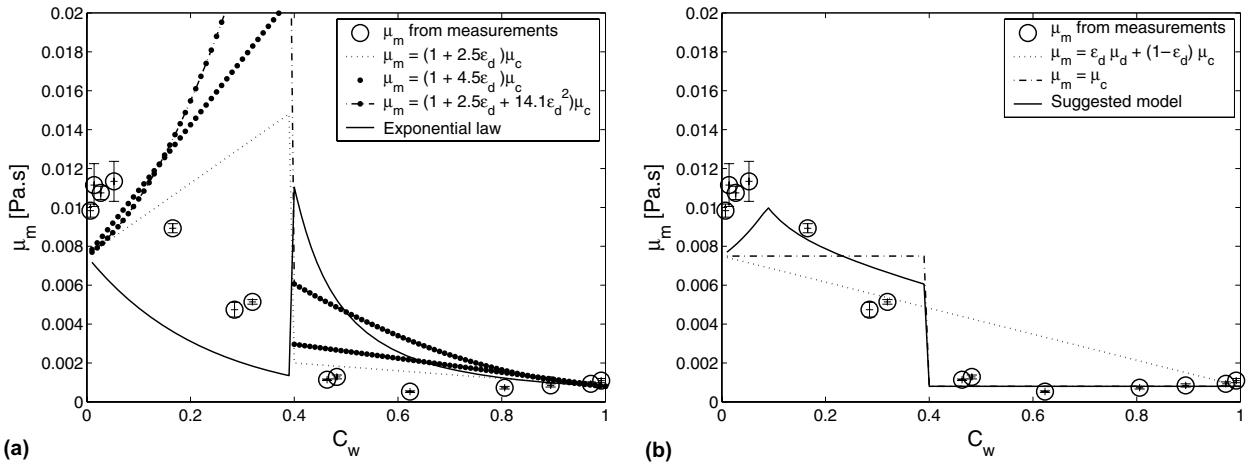

Fig. 5. Comparison between the effective viscosity estimates and correlations [1]–[6]. (a) Comparison with models [1]–[4]; (b) comparison with models [5] and [6], and with our new hybrid model.

3. $\mu_m = (1 + 2.5\epsilon_d + 14.1\epsilon_d^2)\mu_c$, an extension of the model of Einstein (1906) valid for dispersed fractions of up to $\epsilon_d \approx 0.1$ (Becher, 2001);
4. An exponential law, using $\mu_m = \mu_c e^{k_1 \epsilon_d}$, where k_1 is a fitting parameter, e.g., $k_1 = -4.4$ for water in oil dispersion and $k_1 = 2.5$ for oil in water dispersion (see Brauner (1998) for an overview of available exponential-law viscosity models);
5. $\mu_m = \mu_c$, i.e., the continuous phase viscosity is considered;
6. $\mu_m = \epsilon_d \mu_d + (1 - \epsilon_d)\mu_c$, a linear average model for the effective viscosity (Elseth, 2001).

The inversion from oil continuous to water continuous also has to be taken into account in these models. For this purpose, the critical water cut $C_{w,crit}$ for the inversion from water in oil dispersion to oil in water dispersion is taken from Arirachakaran et al. (1989) (Eq. (2)). As illustrated by Fig. 5a and b, the mixture viscosity values cannot be closely described with these models taken from literature. Among these models, the simple model [5] based on the continuous phase viscosity gives the best comparisons. However, although it correctly predicts the dispersion of oil in water conditions, the comparisons in oil continuous flow, i.e., for $C_w < C_{w,crit}$, are relatively poor.

The approach used here to develop a new effective viscosity model is based on a comparison of our experimental data with existing models, and considerations on the maximum drop size. In our flow conditions, the maximum drop size can be expected to have varied significantly from one experiment to the other, due to a competition between drop break-up due to turbulence and drop coalescence at increased water cut. The drop size can be expected to be much smaller when operating at dispersed phase volume fraction lower than $\epsilon_{d,c} \approx 0.089$ since in this regime, drop break-up is the dominant effect (see Appendix A and Brauner (2001)).

The maximum drop size can be estimated by applying the models used in the flow-pattern map criteria (Eqs. (A.2) and (A.3)). Applying this maximum drop size model to our experimental data for estimating the maximum size of the drops present in our system leads to $d_{max} \approx 0.5 - 1.5$ mm for low dispersed fractions (i.e, $C_w < 0.089$ or $C_w > 0.911$), and $d_{max} \approx 0.5 - 6$ mm for $0.089 < C_w < 0.911$. It can therefore be expected that for low dispersion concentration, an emulsion model for the effective viscosity will be valid, while for increased dispersion concentration a large drop model, such as the continuous phase or a linear average formulation, will give a better description of the effective viscosity. This explains the increasing effective viscosity with increased water cut for $C_w < 0.1$ (where the drop size is decreasing), and the decreasing effective viscosity for $0.1 < C_w < 0.4$ (where the drop size is increasing due to coalescence).

In the spirit of the model suggested by Pan et al. (1995) and in view of the measurements, we suggest the use of an hybrid water-cut dependent model.

- For a dispersion of water in oil ($C_w < C_{w,crit}$) the dispersed phase volume fraction is approximated by $\epsilon_d = C_w$:
  - if $\epsilon_d < \epsilon_{d,c}$, the appropriate mixture viscosity is an emulsion model (Becher, 2001):

$$\mu_m = (1 + 2.5\epsilon_d + 14.1\epsilon_d^2)\mu_c, \tag{7}$$

  - if $\epsilon_d > \epsilon_{d,c}$, coalescence is playing an important role and the maximum drop size is significantly increased. Assuming that an excess of large drops is present at a fraction $\epsilon_{d,e}$ which can be estimated to first order by $\epsilon_{d,e} = \epsilon_d - \epsilon_{d,c}$,

$$\mu_m = [(1 + 2.5\epsilon_{d,c} + 14.1\epsilon_{d,c}^2)\mu_c](1 - \phi) + [\epsilon_{d,e}\mu_d + (1 - \epsilon_{d,e})\mu_c]\phi, \tag{8}$$

    in which ϕ is an indication of the relative fraction of large drops present in the mixture. As a first approximation, it is estimated by

$$\phi = \frac{\epsilon_d - \epsilon_{d,c}}{\epsilon_d}. \tag{9}$$

- For a dispersion of oil in water ($C_w > C_{w,crit}$), we use the continuous phase viscosity, i.e., $\mu_m = \mu_w$, since, as discussed before, in those conditions the effective viscosity does not change significantly with C_w.

This new hybrid model is plotted with the experimental data in Fig. 5b. As illustrated by this figure our new hybrid viscosity model describes reasonably the measurements. It should however be noticed that our model displays a discontinuity at the phase inversion, which does not appear on the experimental data. Detailed measurements at the onset of phase inversion would be of support to study the validity of the model in these conditions.

7. Pressure gradient predictions

In the present research we are particularly interested in making realistic pressure gradient predictions, since it would enable us to solve the inverse problem. It is therefore of interest to investigate which effective viscosity model gives the best accuracy with respect to the pressure gradient predictions. The pressure gradient is modelled by using

$$\left[\frac{\partial P}{\partial z}\right] = \left[\frac{\partial P}{\partial z}\right]_g + \left[\frac{\partial P}{\partial z}\right]_f, \tag{10}$$

where the gravitational part $\left[\frac{\partial P}{\partial z}\right]_g = \rho_m g \sin\beta$ is obtained by using the mixture density data and $\left[\frac{\partial P}{\partial z}\right]_f = \frac{f\rho_m U_m^2}{2D}$ is computed by using the measured volumetric flow rates to estimate U_m. Different effective viscosity correlations

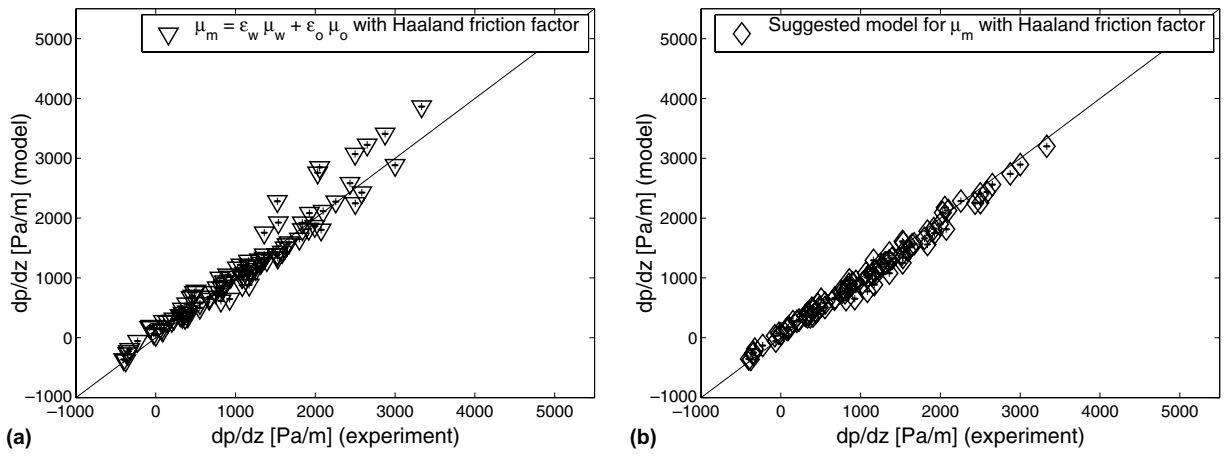

Fig. 6. Predicted pressure gradient with two different models for the effective viscosity: (a) linear average mixture viscosity model [6]; (b) suggested hybrid viscosity model. The relation of Haaland (1983) is used for the friction factor.

were implemented in the friction factor model of Haaland (1983). Two different models for the effective viscosity are tested in Fig. 6a and b. From these pressure gradient prediction results, it is clear that the model based on the linear average viscosity $\mu_m = \epsilon_d\mu_d + (1-\epsilon_d)\mu_c$ does not give satisfying results (Fig. 6a). Using our hybrid model for the effective viscosity permits to significantly improve the pressure gradient predictions (Fig. 6b). Therefore, our hybrid model for the effective viscosity will be used in the following sections.

8. An inverse model for the dispersed flow regime

In this section an inverse model is proposed for the reconstruction of oil and water flow rates from pressure gradient and mixture density information, provided the flow regime is found to be in the dispersed regime and the effective viscosity of the dispersion can be described with the models suggested above. We will also consider the possibility of determining the flow regime with the inverse model. First, the quantities of input are listed. Then the inverse modelling approach, also called inverted model, is described. The results obtained by applying this approach to our data are compared with direct measurements of phase flow rates.

8.1. Input parameters

The quantities of input are:

- The area-average mixture density ρ_m, obtained experimentally via gamma-ray measurements with an accuracy of $\pm 0.87\%$,
- the axial pressure gradient, $\left[\frac{\partial P}{\partial z}\right]$, measured via differential pressure meters. The associated accuracy is $\pm 0.2\%$.

8.2. Reconstruction method

Based on the measured values of ρ_m and $\left[\frac{\partial P}{\partial z}\right]$, the following reconstruction scheme is applied:

1. First, we assume that the flow regime is dispersed and that the homogeneous no-slip model may be applied. Then, the measured mixture density ρ_m provides direct information on the water cut:
$$C_w = \frac{\rho_m - \rho_o}{\rho_w - \rho_o}, \tag{11}$$
in which the density of the oil and of the water are known quantities.
2. Based on the critical value of C_w as proposed by Arirachakaran et al. (1989), the flow is determined as dispersed oil in water or dispersed water in oil.
3. The continuous phase being known, the effective viscosity is determined on the basis of our model.
4. With the above information and the measured pressure gradient, the mixture velocity can be determined:
$$fU_m^2 = \frac{2D}{\rho_m}\left[\rho_m g \sin\beta - \frac{\partial P}{\partial z}\right]. \tag{12}$$
The value of the mixture velocity satisfying Eq. (12) is solved iteratively for each experimental data point, since the value of U_m should also be considered in the friction factor relation f of Haaland (1983).
5. The superficial velocities of oil and of water are then calculated from $U_{sw} = C_w U_m$ and $U_{so} = (1-C_w)U_m$.
6. Finally, the reconstructed values of U_{sw} and U_m are used to filter non-fully dispersed flow regime data points. This filtering is based on the critical superficial velocities obtained with the dispersed flow transition model (Section 2.1).

8.3. Expected intrinsic accuracy of the reconstruction method

This suggested method and the results for the pressure gradient (Rodriguez and Oliemans, 2006) illustrate an important issue for the accuracy of the reconstruction method: since the frictional pressure gradient is

obtained by a difference between two terms (the overall pressure gradient and the gravitational part), the accuracy of the reconstructed superficial velocities is a result of the accuracy of the measurement techniques and of the flow conditions. To evaluate this error, the effects of the pressure gradient and gamma-ray densitometry measurement accuracy on the precision of the reconstructed velocities are also computed: our reconstruction method is applied by using possible extremum values taken by the mixture density and pressure gradient for each data point (Eqs. (11) and (12) are used for error-propagation purpose). The resulting intrinsic error can then be estimated by comparing the results for the reconstructed velocities.

In our flow conditions and with our measurement techniques, values for this intrinsic error of the method are less than $\pm 10\%$ for the mixture velocity and $\pm 25\%$ for the phases superficial velocities in horizontal flow. In practical operating flow conditions this intrinsic error can be obtained in the same way by using the measuring instrument accuracies. It can also be complemented by other error sources (e.g., an error on the inclination angle of the pipe, or on the fluid properties), and can be used as a tool for deciding if the method can be applied with enough accuracy. In the present study these error propagations due to measurement techniques are represented by errorbars on the results for the reconstructed velocities.

8.4. Results: comparison with experiments

The results obtained by applying this approach to our collected experiments are presented in this section. To validate our inverse model, these results are compared with the direct measurements of oil and of water flow rates for all pipe inclinations.

8.4.1. Mixture velocity reconstruction

We computed the results for the mixture velocity by using the measured mixture density and pressure gradients in Eq. (12). We then applied the dispersed flow regime transition criterion given by step 6 above. The filtered mixture velocity results are then compared with the corresponding direct measurements of the mixture velocity. These results are displayed in Fig. 7a for $\beta = 0$ and in Fig. 7b for all inclination angles. The errorbars represent the error propagation related to the pressure gradient and gamma-ray measurement techniques. The mixture velocity values are properly reconstructed by using our method: the mean relative deviation from the measurements $\frac{\Delta U_m}{U_m}$ is 2.5% for $\beta = 0$ and 6.9% when using all inclination angles. The associated maximum deviations are 6% (for $\beta = 0$) and 40% (for all inclinations).

Applying our reconstruction method based on the homogeneous no-slip model assumptions to stratified flow data may lead to misleading estimates of the superficial velocity. In principle, these reconstructed stratified flow superficial velocities might therefore be overestimated, and be taken as dispersed flow experimental

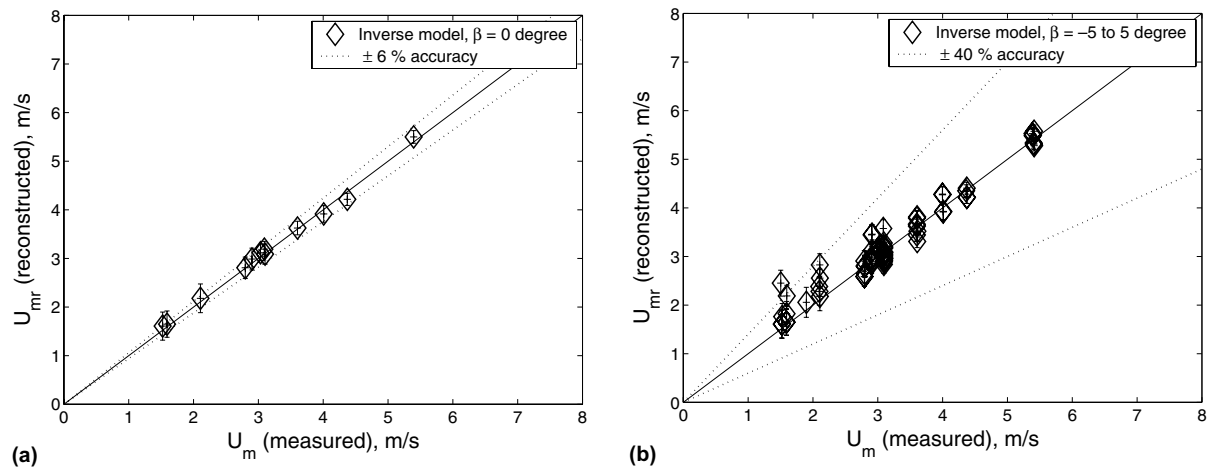

Fig. 7. Mixture velocity estimates based on the reconstruction method, as a function of the measured mixture velocity, (a): for $\beta = 0$; (b): for various values of the inclination angle β. The bisector is also shown.

data in step 6 of the reconstruction method. In that respect it is interesting to note that 86 points were found, while the direct application of this criterion to the flow rate measurements leads to 90 selected experiments. Analysing the selected data points with the collected movies showed that among these 86 selected points 85 are, as expected, dispersed flow regime data points. Only one data point was corresponding to non-dispersed flow conditions. This is a good indication that, in the frame of the present inverse method, the 'à posteriori' determination of the flow pattern based on the reconstructed superficial velocities does not lead to excessive misinterpreted results.

8.4.2. Oil and water superficial velocities

The oil and water superficial velocity reconstructions are compared with their direct measurements at $\beta = 0$ in Fig. 8a and b. The phase velocities are surprisingly well reconstructed in that case. The maximum deviations from the measurements are 13% on the superficial oil velocity and 17% on the superficial water velocity. The mean deviations are $\frac{\Delta U_{so}}{U_{so}} = 4.3\%$ and $\frac{\Delta U_{sw}}{U_{sw}} = 12.2\%$. In Fig. 9a and b, the comparisons for the superficial oil and water velocity reconstructions are shown for all inclination angles. The accuracy of the method is significantly decreased when analysing slightly inclined flow conditions. In this case the maximum deviations are typically 50% for the oil and water superficial velocities. The mean deviations from the direct measurements are $\frac{\Delta U_{so}}{U_{so}} = 9.6\%$ and $\frac{\Delta U_{sw}}{U_{sw}} = 26\%$.

These comparisons clearly illustrate that the contribution of gravity to the pressure measurements has an important impact on the accuracy of the method. This was also observed by analysing the error propagation for inclined flow situations. In addition these slight inclination angles might result in some flow and phase heterogeneities, which are not taken into account with a homogeneous no-slip model. When comparing the gamma-ray measurements for the mixture density with homogeneous no-slip assumption calculations, we also observed that the measurements for $\beta = 0$ provided better comparisons than the measurements made at slight inclination. This observation supports the idea that radial phase distribution effects may start to play a role in slightly inclined flow conditions. Local measurements could be of support to clarify these expectations.

Comparisons of the present inverse method were also made with the experimental data reported by Angeli and Hewitt (1998). In this case typical deviations between the reconstructed oil and water superficial velocities and the measurements were of $\frac{\Delta U_s}{U_s} \approx 15\%$ for steel pipe flow conditions and of $\frac{\Delta U_s}{U_s} \approx 22\%$ for acrylic pipe flow conditions. As reported by the authors, when using the acrylic pipe it was observed that the wall was preferentially wetted by oil, while no preference was observed for the steel pipe. The difference between the acrylic and the steel pipe flow pressure gradient measurements could not be explained only in terms of the difference in tube roughness. Therefore, an interesting improvement of the present method would be to include considerations on the pipe wettability in the frictional pressure gradient model.

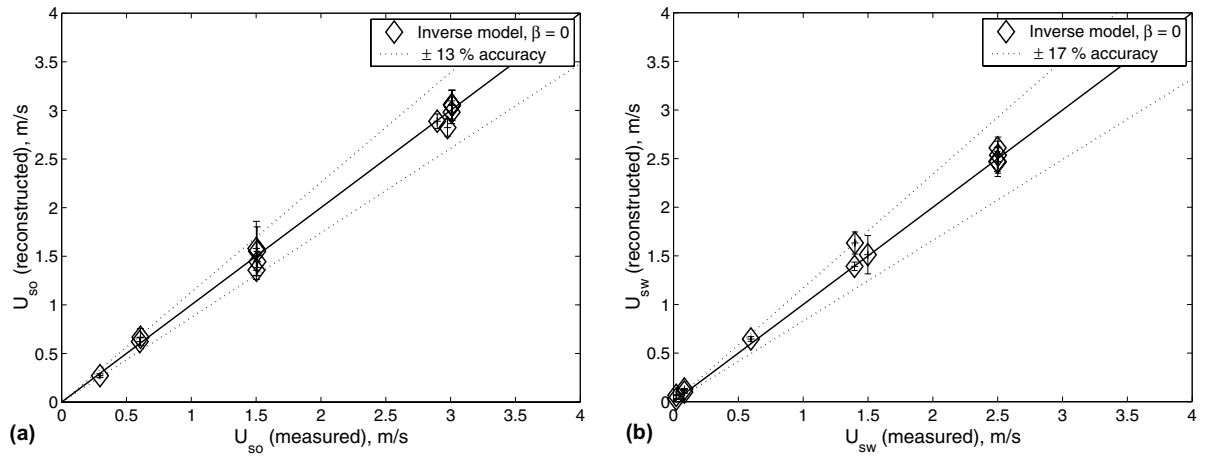

Fig. 8. Oil and water superficial velocity estimates based on the reconstruction method, as a function of the measured values for $\beta = 0$. The bisector is also shown.

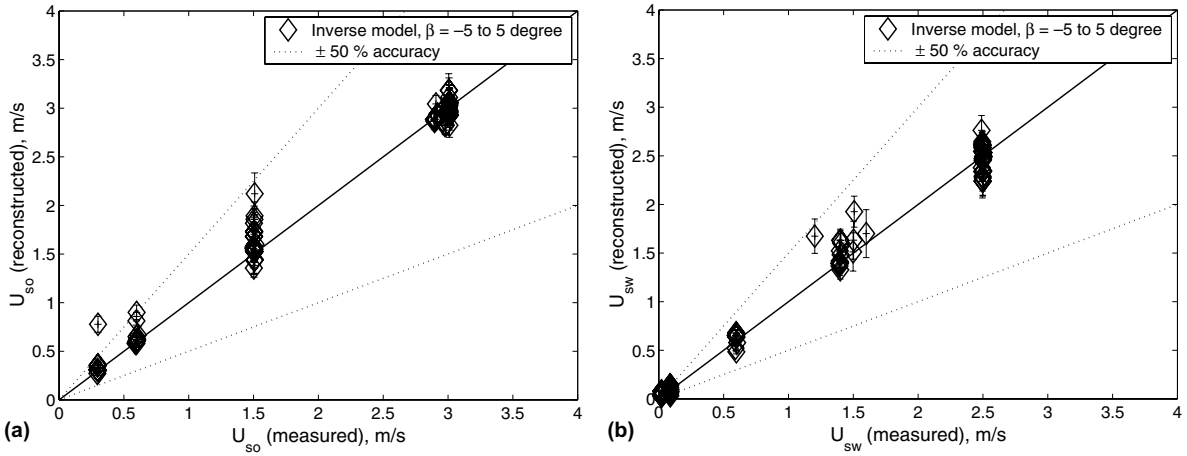

Fig. 9. Oil and water superficial velocity estimates based on the reconstruction method, as a function of the measured values for various values of the inclination angle β. The bisector is also shown.

9. Conclusions and recommendations

In this study we implemented the physically based model developed by Brauner (2001) for the transition from separated flow to dispersed flow in horizontal and slightly inclined oil–water pipe flows. This model was subsequently extended to take into account wall roughness effects. A set of experimental data collected on a pipe of diameter $D = 82.8$ mm and of length $L = 15$ m at various (small) deviation angles from the horizontal has been used for the analysis of flow pattern, pressure gradient and water cut data (Rodriguez and Oliemans, 2006). The flow pattern model implemented in this study was shown to describe satisfactorily the flow regime transition for our own experiments and for experiments collected at various pipe diameters and fluid properties conditions. This physically based model permits to describe the effect of pipe inclination. It can also give interesting indications on the effect of wall roughness and flow conditions on the maximum drop size.

From the experimental results, flow conditions corresponding to the dispersed flow regime have been selected. These data correspond to 90 experimental points, i.e., approximately 15 data points per inclination angle. The existence of the dispersed flow regime for these data points was further confirmed by visual observations of the digital movies recorded during the experiments (Rodriguez and Oliemans, 2006). In addition the associated mixture density data collected via a gamma-ray densitometer confirmed the validity of the homogeneous-no slip model assumption for computing the mixture density in these conditions.

Information on the effective viscosity has been extracted from the measurements. The effective viscosity changes with water cut could not be described satisfactorily with available correlations. Among available models, the continuous phase viscosity was found to provide the nearest description of our experiments. A new hybrid model for the effective viscosity was suggested, based on considerations on the maximum drop size changes with water cut and available models. The pressure gradient data were correctly described by using this viscosity model in the friction factor law proposed by Haaland (1983) at various angles of inclination (this is clearly illustrated by Fig. 6b, in which all the 90 dispersed flow condition data points are displayed).

A method for evaluating the superficial velocities of oil and of water from mixture density and pressure gradient measurements was then developed for the dispersed flow regime. In general this method was shown to reconstruct the superficial velocities with an accuracy of $\pm 50\%$. When considering only our horizontal dispersed flow experiments, the maximum deviation was reduced to 17%. As a next step, it would be interesting to extend this inverse model to cover other flow regime conditions. Since the inverse model developed in this contribution permits to filter non-dispersed flow regime conditions, it could be used as a first step in a multiple flow-regime inverse modelling approach.

The effective properties of the oil–water mixture used in the present experimental work was determined by using the measured pressure gradient and flow rates. An effective viscosity model was suggested based on

considerations of drop break-up and coalescence effects. In this respect it would also be interesting to study in more detail the changes of effective viscosity with drop size (and drop size distribution) by means of local measurements. Our pressure gradient model could also be improved by considering the effects of pipe material wettability (Angeli and Hewitt, 1998).

Acknowledgements

Financial support was provided by Shell Exploration and Production. Sébastien Guet and Oscar Rodriguez are grateful to Roel Kusters, Hans van den Boer and Arno Van der Handel for their continuous interest and their support in collecting the experimental data on the Donau flow loop, in Shell E&P, Rijswijk, the Netherlands.

Appendix A. Dispersed flow boundaries

A.1. Critical drop size

The critical drop size is given by (Barnea, 1987; Brauner, 2001):

$$d_{\mathrm{crit}} = \min(d_{c\sigma}, d_{cb}), \tag{A.1}$$

where $\frac{d_{c\sigma}}{D} = \frac{0.224}{(\cos(\beta)Eo_D)^{\frac{1}{2}}}$ is the maximum (dimensionless) size for drop deformation ($Eo_D = \frac{\Delta\rho g D^2}{8\sigma}$ is the Eötvös number). $\frac{d_{cb}}{D} = \frac{3}{8}\frac{\rho_c}{\Delta\rho}\frac{fU_m^2}{Dg\cos(\beta)}$ is the critical drop size for migration toward the wall due to gravity. Here the subscript c and d denote the continuous and the dispersed phase and ϵ_d the dispersed phase fraction.

A.2. Maximum drop size

The maximum (dimensionless) drop size existing in a dilute dispersion was modelled by Hinze (1959):

$$\left(\frac{d_{\max}}{D}\right)_0 = 0.55\left(\frac{\rho_c U_m^2 D}{\sigma}\right)^{-0.6}\left[\frac{\rho_m}{\rho_c(1-\epsilon_d)}f\right]^{-0.4}. \tag{A.2}$$

Brauner (2001) extended this approach to dense dispersions. In that case coalescence also has to be taken into account for the determination of the maximum drop size. This extended model is given by

$$\left(\frac{d_{\max}}{D}\right)_\epsilon = 2.22C_H^{\frac{3}{5}}\left(\frac{\rho_c U_m^2 D}{\sigma}\right)^{-0.6}\left[\frac{\rho_m}{\rho_c(1-\epsilon_d)}f\right]^{-0.4}\left(\frac{\epsilon_d}{1-\epsilon_d}\right)^{0.6}, \tag{A.3}$$

where the coefficient C_H is a proportionality coefficient describing the amount of turbulent kinetic energy available for drop-break-up (we use $C_H = 1$, see Brauner (2001)).

The maximum possible drop size in the system is the maximum value:

$$\frac{d_{\max}}{D} = \mathrm{Max}\left[\left(\frac{d_{\max}}{D}\right)_0, \left(\frac{d_{\max}}{D}\right)_\epsilon\right]. \tag{A.4}$$

The flow pattern is known to be fully dispersed when turbulence break-up determines the maximum drop size existing in the system. Following the above mentioned models, it is determined by

$$\mathrm{Max}\left[\left(\frac{d_{\max}}{D}\right)_0, \left(\frac{d_{\max}}{D}\right)_\epsilon\right] = \min(d_{c\sigma}, d_{cb}). \tag{A.5}$$

A.3. Model extension

In the present model, the formulation is extended to take into account the effects of wall roughness. The correlation of Haaland (1983) for the friction factor is used for this purpose (Eq. (1)). Using this relation the maximum drop size is written as

$$\mathrm{Max}\left[\left(\frac{d_{\max}}{D}\right)_0,\left(\frac{d_{\max}}{D}\right)_\epsilon\right]=C_{1r}f^{-0.4}U_{\mathrm{m}}^{-1.2}, \tag{A.6}$$

where C_{1r} is given by

$$C_{1r}=\left(\frac{\rho_{\mathrm{c}}D}{\sigma}\right)^{-0.6}\left[\frac{\rho_{\mathrm{m}}}{\rho_{\mathrm{c}}(1-\epsilon_{\mathrm{d}})}\right]^{-0.4}\mathrm{Max}\left[0.55,2.22C_H^{\frac{3}{5}}\left(\frac{\epsilon_{\mathrm{d}}}{1-\epsilon_{\mathrm{d}}}\right)^{0.6}\right]. \tag{A.7}$$

The change from low dispersed fraction to large fraction is taken into account by the Max function. It occurs at a critical value of the dispersed phase fraction $\epsilon_{\mathrm{d}}=\epsilon_{\mathrm{d,c}}$ corresponding to $2.22C_H^{\frac{3}{5}}\left(\frac{\epsilon_{\mathrm{d,c}}}{1-\epsilon_{\mathrm{d,c}}}\right)^{0.6}=0.55$. Assuming $C_H=1$, the critical dispersed phase fraction value is $\epsilon_{\mathrm{d,c}}=0.089$.

The critical dimensionless drop size is given by

$$\frac{d_{\mathrm{crit}}}{D}=\min(C_{2r},C_{3r}fU_{\mathrm{m}}^2), \tag{A.8}$$

where $C_{2r}=C_{2s}=d_{\mathrm{c}\sigma}$ and $C_{3r}=\frac{3}{8}\frac{\rho_{\mathrm{c}}}{\Delta\rho}\frac{1}{D_{\mathrm{p}}g\cos(\beta)}$ are constants for a given oil–water system.

A.4. Model implementation

An iteration on ϵ_{d} is done, ϵ_{d} is varied from $\epsilon_{i=1}=0$ to $\epsilon_{i=N}=\epsilon_{\mathrm{inv}}$ corresponding to the critical liquid fraction for phase inversion as proposed by Arirachakaran et al. (1989). For each value of ϵ_i, the constants C_{1r}, C_{2r} and C_{3r} are computed and the mixture velocity $U_{\mathrm{m}}=U_{\mathrm{mb}}$ associated with $d_{\mathrm{cb}}=d_{\max}$ is determined by solving

$$f^{1.4}U_{\mathrm{m}}^{3.2}-\frac{C_{1r}}{C_{3r}}=0. \tag{A.9}$$

This equation is solved by using numerical iteration. Then, $d_{\mathrm{cb}}=C_{3r}fU_{\mathrm{mb}}^2$ and $d_{\mathrm{c}\sigma}=C_{2r}$ are compared. If $d_{\mathrm{cb}}<d_{\mathrm{c}\sigma}$ then the critical mixture velocity associated with flow pattern transition is given by $U_{\mathrm{mr,fp}}=U_{\mathrm{mb}}$. Otherwise, $U_{\mathrm{mr,fp}}$ is determined via the value of $U_{\mathrm{m}\sigma}$ associated with $d_{\mathrm{crit}}=d_{\mathrm{c}\sigma}$. The mixture velocity $U_{\mathrm{m}}=U_{\mathrm{m}\sigma}$ associated with $d_{\mathrm{c}\sigma}=d_{\max}$ is determined numerically by solving

$$f^{-0.4}U_{\mathrm{m}}^{-1.2}-\frac{C_{2r}}{C_{1r}}=0. \tag{A.10}$$

Finally, the superficial velocities of the dispersed and of the continuous phase at flow pattern transition are computed according to

$$U_{\mathrm{sd}}=\epsilon_{\mathrm{d}}U_{\mathrm{mr,fp}}, \tag{A.11}$$

and

$$U_{\mathrm{sc}}=(1-\epsilon_{\mathrm{d}})U_{\mathrm{mr,fp}}. \tag{A.12}$$

References

Angeli, P., Hewitt, G.F., 1998. Pressure gradient in horizontal liquid–liquid flows. Int. J. Multiphase Flow 24, 1183–1203.

Arirachakaran, S., Oglesby, K.D., Malinowsky, M.S., Shoham, O., Brill, J.P., 1989. An analysis of oil/water flow phenomena in horizontal pipes. SPE paper 18836. SPE Prof. Prod. Operating Symp., Oklahoma.

Barnea, D., 1987. A unified model for predicting flow pattern transitions for the whole range of pipe inclinations. Int. J. Multiphase Flow 13, 1–12.

Becher, P., 2001. Physical Properties of Emulsions. American Chemical Society, Washington.

Brauner, N., 1998. Liquid–liquid two-phase flow. In: HEDU – Heat Exchanger Design Update. pp. 1–40 (Chapter 2.3.5).

Brauner, N., 2001. The prediction of dispersed flow boundaries in liquid–liquid and gas–liquid systems. Int. J. Multiphase Flow 27, 885–910.

Brauner, N., Ullmann, A., 2002. Modeling of phase inversion phenomenon in two-phase pipe flows. Int. J. Multiphase Flow 28, 1177–1204.

Decarre, S., Fabre, J., 1997. Etude sur la prédiction de l'inversion de phase. Rev. IFP 52, 415–424.

Einstein, A., 1906. Eine Neue Bestuimmung Der Molekulardimensionen. Ann. Phys. 9, 289–306.

Elseth, G., 2001. An experimental study of oil/water flow in horizontal pipes. PhD thesis, NTNU Trondheim, Norway.

Fairusov, Y.V., Arenas-Medina, P., Verdejo-Fierro, J., Gonzales-Islas, R., 2000. Flow pattern transitions in horizontal pipelines carrying oil–water mixtures: full-scale experiments. J. Energ. Resour. Technol. 122, 169–175.

Haaland, J., 1983. Simple and explicit formulae for the friction factor in turbulent pipe flow. J. Fluid Eng. 105, 89–90.

Hinze, J., 1959. Turbulence. McGraw-Hill, New York.

Pal, J., 2001. Novel viscosity equations for emulsions of two immiscible liquids. J. Rheol. 45, 509–519.

Pan, L., Jayanti, S., Hewitt, G.F., 1995. Flow patterns, phase inversion and pressure gradient in air–oil–water flow in horizontal pipe. In: Proceedings of the Second International Conference on Multiphase Flow, April 3–7, Kyoto, Japan.

Rodriguez, O.M.H., Oliemans, R.V.A., 2006. Experimental study on oil–water flow in horizontal and slightly inclined pipes. Int. J. Multiphase Flow 32, 323–343.

van Kemenade, E., Mondt, E., Verbeek, P., 2003. Liquid-phase separation with rotational particle separator. Chem. Eng. Technol. 26, 1176–1183.